AGU PUBLICATIONS

Geophysical Research Letters

RESEARCH LETTER
10.1002/2017GL075472

Key Points:
- Late summer frazil ice-associated algal blooms are concentrated in major sea ice production polynyas
- Green colored frazil ice is present over more than 300,000 km^2 during March
- Satellite observations show substantial interannual variability in green colored frazil ice extent

Supporting Information:
- Supporting Information S1

Correspondence to:
H. B. DeJong,
hdejong@stanford.edu

Citation:
DeJong, H. B., Dunbar, R. B., & Lyons, E. A. (2018). Late summer frazil ice-associated algal blooms around Antarctica. *Geophysical Research Letters*, *45*, 826–833. https://doi.org/10.1002/2017GL075472

Received 28 AUG 2017
Accepted 30 DEC 2017
Accepted article online 4 JAN 2018
Published online 17 JAN 2018

Late Summer Frazil Ice-Associated Algal Blooms around Antarctica

Hans B. DeJong[1], Robert B. Dunbar[1], and Evan A. Lyons[1]

[1]Department of Earth System Science, Stanford University, Stanford, CA, USA

Abstract Antarctic continental shelf waters are the most biologically productive in the Southern Ocean. Although satellite-derived algorithms report peak productivity during the austral spring/early summer, recent studies provide evidence for substantial late summer productivity that is associated with green colored frazil ice. Here we analyze daily Moderate Resolution Imaging Spectroradiometer satellite images for February and March from 2003 to 2017 to identify green colored frazil ice hot spots. Green frazil ice is concentrated in 11 of the 13 major sea ice production polynyas, with the greenest frazil ice in the Terra Nova Bay and Cape Darnley polynyas. While there is substantial interannual variability, green frazil ice is present over greater than 300,000 km^2 during March. Late summer frazil ice-associated algal productivity may be a major phenomenon around Antarctica that is not considered in regional carbon and ecosystem models.

1. Introduction

Antarctic continental shelves are the most biologically productive regions in the Southern Ocean (Arrigo & McClain, 1994; Arrigo, van Dijken, & Bushinsky, 2008; Arrigo, van Dijken, & Strong, 2015; Smith & Gordon, 1997; Yager et al., 2016) and are disproportionately large atmospheric CO_2 sinks (Arrigo, van Dijken, & Long, 2008; Mu et al., 2014; Sweeney, 2003). During the austral spring, large phytoplankton blooms develop in polynyas (open water surrounded by sea ice), with peak productivity extending through December or early January (Long et al., 2011; Smith & Gordon, 1997; Smith et al., 1996, 2000). Based on satellite chlorophyll estimation, net primary productivity (NPP) in Antarctic polynyas declines during February and approaches zero in March (Arrigo, van Dijken, & Strong, 2015).

Recent studies from Antarctic coastal regions have found evidence for substantial late season primary productivity during February and March. This water column productivity is associated with algal accumulation in frazil ice. Lieser et al. (2015) observed green frazil ice during early March 2012 near Cape Darnley that they estimated was 30,000 km^2. Furthermore, underway fluorometry (5 m depth) showed elevated chlorophyll underneath the green frazil ice. They hypothesized that there was substantial productivity within and underneath the green frazil ice. DeJong et al. (2017) also observed frazil ice in wind-rows in Terra Nova Bay polynya in the western Ross Sea during late February and early March 2013 that over time exhibited green colors from algal accumulation. Based on a time series of nutrient deficits, mixed layer depths, and surface pCO_2 measurements, DeJong et al. (2017) concluded that this frazil ice-associated water column algal bloom was very productive (net community production = 425 ± 204 mmol C m^{-2} d^{-1}).

Late season productivity by frazil ice-associated algal blooms is not captured in satellite-derived NPP estimates (DeJong et al., 2017; Lieser et al., 2015). Chlorophyll algorithms using Moderate Resolution Imaging Spectroradiometer (MODIS) satellite data mask pixels with high ice coverage because ocean color spectral bands saturate over bright targets such as ice (Esaias et al., 1998; Hu, 2011). The Maximum Chlorophyll Index based on the MEdium Resolution Imaging Spectrometer satellite data detects chlorophyll in water with high scatter from suspended sediment or floating ice crystals but also masks pixels with high ice coverage (Gower & King, 2007; Gower & King, 2013).

Frazil ice with high algal concentrations are observed in true color satellite images across many locations around the continent, suggesting that late season productivity may be a major phenomenon (Figure 1). For both Cape Darnley and Terra Nova Bay, frazil ice-associated algal blooms that have been documented in the field are also clearly visible in the corresponding true color satellite images (DeJong et al., 2017; Lieser et al., 2015). Here we use daily MODIS visible spectral band satellite images from 2003 through 2017 to identify green colored frazil ice hot spots and examine interannual variability in green colored frazil ice extent.

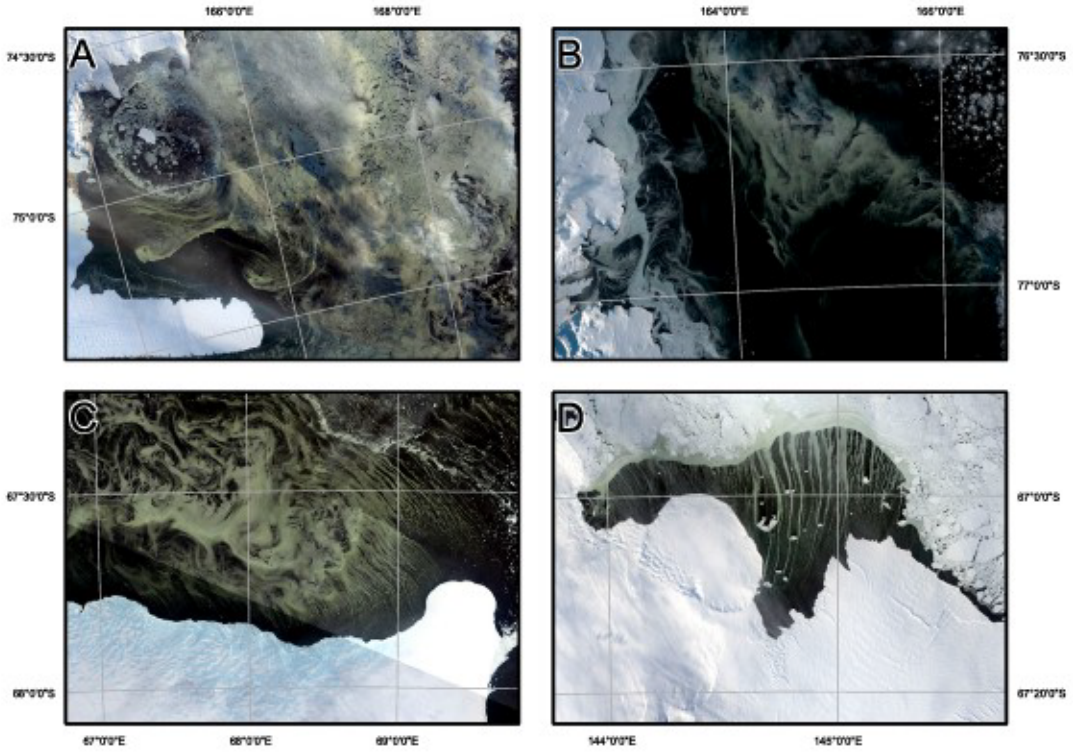

Figure 1. True color (Bands 4, 3, and 2) 30 m resolution Landsat-8 satellite images from (a) Terra Nova Bay polynya on 5 March 2015, (b) Granite Harbor on 5 March 2017, (c) Cape Darnley on 29 February 2016, and (d) Mertz polynya on 4 March 2017.

2. Methods

2.1. MODIS Data

All satellite data were processed using ArcGIS and Interactive Data Language. We used the MODIS Surface Reflectance Daily L2G Global product from both the Terra and Aqua satellites (MOD09GA/MYD09GA Version 006) (Vermote et al., 2015). Surface reflectance is the ratio of surface radiance (at ground level) to surface irradiation and corrects for Sun angle and for the effects of atmospheric gases and aerosols. Since MODIS Surface Reflectance is a land product, tiles are only processed if they include land. We downloaded all MODIS Surface Reflectance tiles for February and March (2003–2017) that include the Antarctic coast (h14-24, v15-16). These tiles cover the majority of the Antarctic continental shelf (Figure 2). We extracted the 500 m visible spectral bands, Band 1 (red = 620–670 nm), Band 3 (blue = 459–479 nm), and Band 4 (green = 545–565 nm), and mosaicked the tiles for each day using a Polar Stereographic Projection.

2.2. Pixel Classification Algorithm

For each day, we determined if a given pixel was green, taken as indicative of algal accumulation in frazil ice. This interpretation is simplified by the fact that scattering of light in frazil ice can be assumed to be wavelength independent in the visible spectrum (Grenfell, 1983, 1991; Perovich, 1996). We masked land and ice shelves with the global, self-consistent, hierarchical, high-resolution shoreline database (Wessel & Smith, 1996) and clouds with the internal 1 km cloud algorithm flag. In addition, pixels were masked if Band 3 or 4 surface reflectance was greater than 100%. Finally, we masked pixels if Band 4 was less than 10% to prevent classifying open water pixels as green and because of the lower signal-to-noise ratio for pixels with low reflectance values. We chose the 10% threshold after experimenting with different thresholds and examining Band 4 surface reflectance histograms (Figures S1 and S2 in the supporting information).

Similar to the normalized difference vegetation index (Rouse et al., 1973), we created a *Green Index* that ranges from −1 to 1:

$$\text{Green Index} = \frac{\text{Band 4} - \text{Band 3}}{\text{Band 4} + \text{Band 3}} \quad (1)$$

Figure 2. Map of Antarctica showing the MODIS Surface Reflectance tiles included in this study (light grey). The five geographical regions (Arrigo, van Dijken, & Bushinsky, 2008) are shown. The major sea ice production polynyas (Tamura et al., 2016) are outlined by the red lines, and the 1,000 m isobath is indicated by the grey line.

We applied the *Green Index* function to nonmasked pixels for each day. Finally, we classified a pixel as green from algal accumulation within frazil ice if the *Green Index* was greater or equal to a threshold. We present the results from three thresholds (0.02, 0.04, and 0.06, hereafter called the lower, medium, and higher thresholds). We combined Terra and Aqua satellite images for each day to maximize the number of cloud free pixels. A pixel was classified as green if that pixel in either Terra or Aqua was green. Similarly, a pixel was classified as cloud-free if that pixel in either Terra or Aqua was cloud-free.

We qualitatively validated our algorithm with 30 m resolution Landsat-8 true color images (Figures S3–S7). The highest threshold captures regions with the greenest frazil ice (e.g., Cape Darnley; Figure S5) but misses some regions where Landsat imagery indicates the presence of green colored frazil ice (e.g., Fimbul Ice Shelf; Figure S7). The lower threshold does a better job capturing regions with less green frazil ice (e.g., Fimbul Ice Shelf; Figure S7).

2.3. Data Analysis

2.3.1. Hot Spot Detection

For each threshold for February and then March of each year, we counted the number of days that each pixel was classified as green. Similarly, we counted the number of days that each pixel was cloud-free. Using these counts, we calculated *Green Frequency* (see Figure S8):

$$\text{Green Frequency} = \left(\frac{\text{number of green days}}{\text{number of cloud free days}}\right) * 100\% \quad (2)$$

Next, we classified pixels as *Monthly Green* if *Green Frequency* was 20% or greater for a particular month. Pixels were masked out if there were fewer than five cloud-free days in a given month. We then calculated *Monthly Green Count*, the number of times a specific pixel was classified as *Monthly Green* between 2003 and 2017

(calculated separately for February and March). We used *Monthly Green Count* to calculate *Percent Years Green* (also calculated separately for February and March):

$$\text{Percent Years Green} = \left(\frac{\text{Monthly Green Count}}{15}\right) * 100\% \quad (3)$$

where 15 is the number of years of data that we analyzed (2003–2017).

To examine the location of green colored frazil ice hot spots, we classified a pixel as a hot spot pixel if *Percent Years Green* was equal or greater than 40%. Finally, we classified a region as a hot spot if it was composed of more than 500 km^2 of connected hot spot pixels (using 8-connected pixel neighborhood criteria).

2.3.2. Interannual Variability

To examine interannual variability, we calculated *Green Frazil Ice Extent* (area of the *Monthly Green* pixels) for February and March of each year. We also calculated *Green Frazil Ice Extent* separately for five geographical sectors (following Arrigo, van Dijken, & Long, 2008; Figure 2). Finally, we evaluated the linear relationship between *Green Frazil Ice Extent* and the Southern Annular Mode (SAM) (Marshall, 2003), El Niño–Southern Oscillation (ENSO) (Wolter & Timlin, 1993, 1998), and Southern Oscillation Index (SOI, www.ncdc.noaa.gov/teleconnections/enso/indicators/soi/).

3. Results and Discussion

3.1. Green Colored Frazil Ice Hot Spots

Green colored frazil ice hot spots are concentrated almost exclusively within the 13 major sea ice production polynyas defined by Tamura et al. (2016) (Figures 3 and S9). The greenest frazil ice hot spots (higher threshold) are found in Terra Nova Bay and Cape Darnley polynyas (Figures 3a and 3b). Using the medium threshold, green colored frazil ice hot spots are found in seven of the major ice production polynyas (Figures 3c and 3d). Finally, based on the lower threshold, green colored frazil ice hot spots are found in 11 of the 13 major sea ice production polynyas. In addition, some green colored frazil ice hot spots are found in smaller ice production regions mainly along the Antarctic coast (Figures 3e and 3f).

DeJong et al. (2017) observed high water column net community production (425 ± 204 mmol C m^{-2} d^{-1}) in Terra Nova Bay during late February and early March 2013 that was associated with green frazil ice in windrows. The strongest katabatic winds in the Ross Sea occur in Terra Nova Bay starting mid-February and prevent the formation of more opaque ice (Arrigo, Weiss, & Smith, 1998; Bromwich, 1989; Parish & Bromwich, 1987; Sanz Rodrigo et al., 2013). DeJong et al. (2017) hypothesized that these strong katabatic winds mixed trace nutrients into the surface from below and caused Langmuir circulation that concentrated algae and frazil ice into discrete rows. The buoyant properties of frazil ice crystals may have kept algae near the surface for longer periods of time, a factor likely to be of greater importance during the late summer when Sun angles are low. In short, we hypothesize that the green colored frazil ice at other locations also represents active phytoplankton growth during the late summer.

The observation of green colored frazil ice hot spots concentrated in the major sea ice production polynya regions supports the hypothesis by DeJong et al. (2017) that late season productivity is ultimately caused by strong katabatic winds. In most major ice production regions, strong katabatic winds continuously advect newly forming sea ice away from the coast. We emphasize that the greenest hot spots (Terra Nova Bay and Cape Darnley/Mackenzie polynyas) occur in regions with some of the highest rates of ice production per unit area (Tamura et al., 2016). These are also important Antarctic Bottom Water production regions (Jacobs et al., 1970; Ohshima et al., 2013; Orsi et al., 1999).

3.2. Green Colored Frazil Ice Extent

Late summer phytoplankton blooms associated with frazil ice may account for substantial productivity that is not included in regional models. In February, green colored frazil ice covers on average 24,000; 81,000; and 425,000 km^2 (higher, medium, and lower thresholds). In March, green colored frazil ice covers on average 108,000; 338,000; and 1,108,000 km^2.

The medium threshold most likely best captures regions with frazil ice-associated algal blooms. During the late summer of 2013, DeJong et al. (2017) found that late season phytoplankton blooms associated with frazil ice were concentrated in Terra Nova Bay polynya. Since the lower threshold classifies the majority of pixels

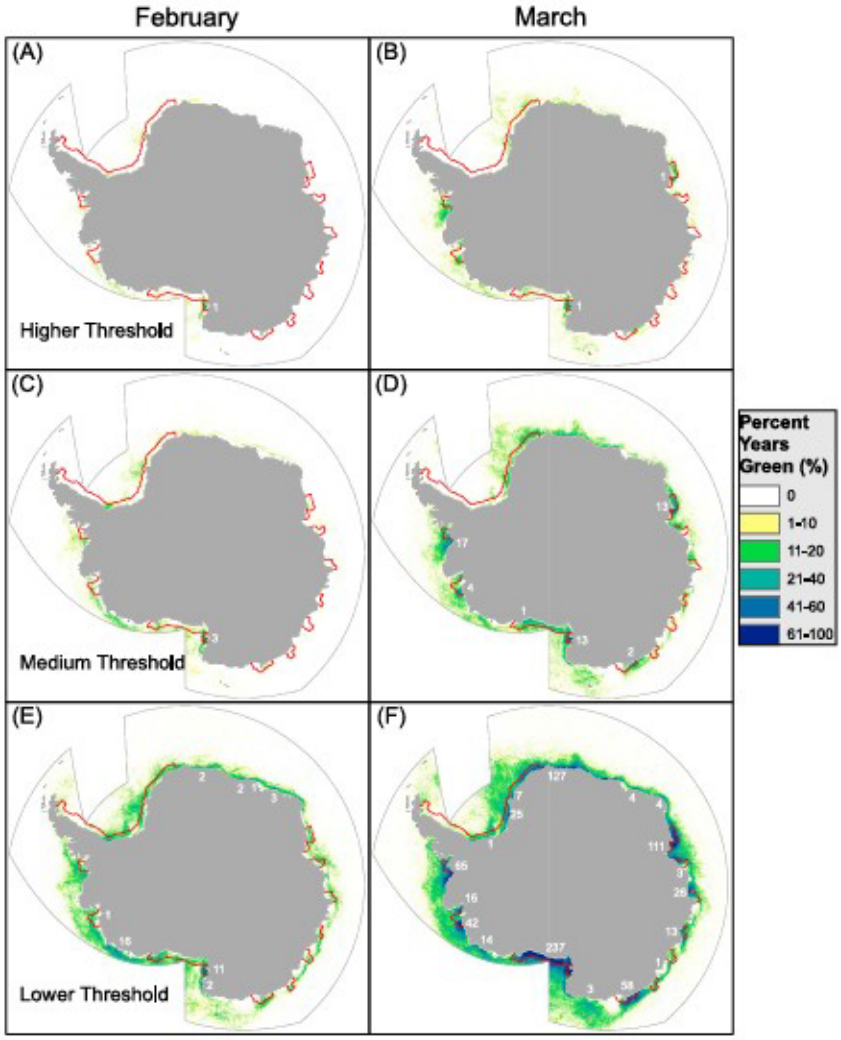

Figure 3. *Percent Years Green* (February and March 2003–2017) based on the (a and b) higher threshold, (c and d) medium threshold, and (e and f) lower threshold. The areas (10^3 km^2) of the green frazil ice hot spots are labeled (white numbers). The major sea ice production polynyas (Tamura et al., 2016) are outlined by the red lines.

across the Ross Sea during March 2013 as *Monthly Green* (Figure S8), it likely overestimates the extent of frazil ice-associated algal blooms. Both the medium and higher thresholds show that *Monthly Green* pixels are concentrated near Terra Nova Bay during March 2013. However, the higher threshold misses large regions where Landsat imagery indicates the presence of green colored frazil ice (e.g., Figures S6 and S7).

The medium threshold suggests that green frazil ice is a major phenomenon. For instance, if average late season productivity in green frazil ice regions during the second half of February and the first half of March is 100 mmol C m^{-2} d^{-1}, which is fourfold lower than reported by DeJong et al. (2017), total production for these 30 days would be 7.6 Tg C based on the medium threshold (*Green Frazil Ice Extent*: February = 81,000 km^2 and March = 338,000 km^2). For comparison, Arrigo, van Dijken, and Strong (2015) estimates with satellite chlorophyll that total NPP on Antarctic continental shelves is 45.6 Tg C yr^{-1}. Our results suggest that late summer productivity is spatially expansive, may be a significant fraction of total shelf productivity, and will provide substantial food for the ecosystem right before the dark winter. Future studies should measure late summer net community productivity rates in both the greenest and least green polynyas.

Late summer frazil ice-associated algal blooms may also substantially enhance the flux of atmospheric CO_2 into the Antarctic continental shelf, especially Antarctic Bottom Water formation regions. DeJong and Dunbar (2017) found that the annual CO_2 flux rate into Terra Nova Bay polynya (3.2 mol C m^{-2} yr^{-1}) is

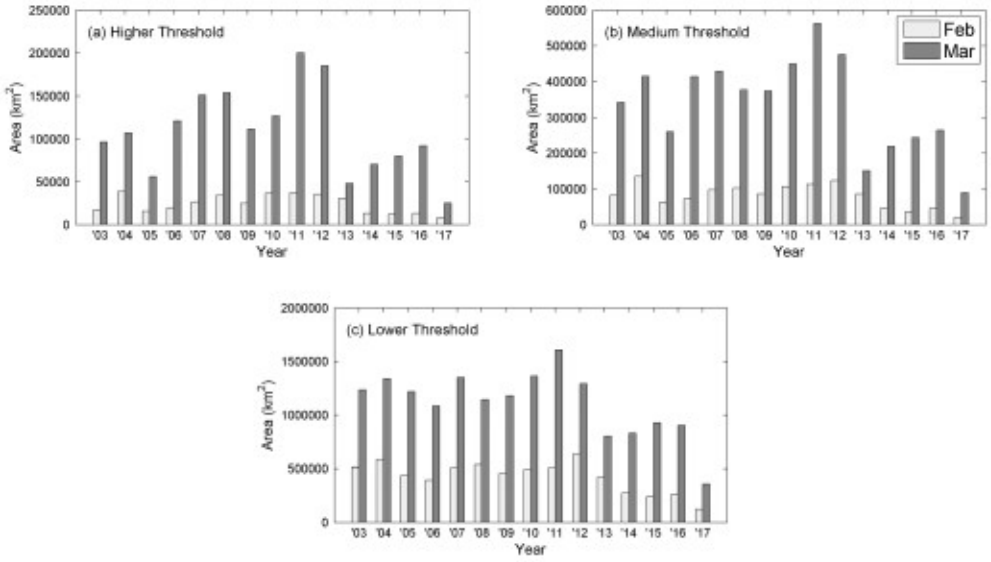

Figure 4. *Green Frazil Ice Extent* (February and March 2003–2017) for the total study region based on the (a) higher threshold, (b) medium threshold, and (c) lower threshold.

twice as high as the mean Ross Sea flux (1.3 mol C m^{-2} yr^{-1}). They attribute the higher CO_2 flux rates into Terra Nova Bay polynya to late summer productivity that kept surface pCO_2 levels low even though strong katabatic winds deepened the mixed layer and entrained CO_2-rich water from below. The unique coupling of gale force winds and low pCO_2 led to extraordinary CO_2 flux rates. If we assume that green frazil ice covers 223,000 km^2 of Antarctic coastal waters (medium threshold, average of February and March) and enhances air to sea CO_2 flux by 1.5 mol C m^{-2}, total Antarctic margin air to sea CO_2 flux would be enhanced by 4 Tg C yr^{-1}. For comparison, the entire Ross Sea annual CO_2 sink is 7.5 Tg C yr^{-1} (DeJong & Dunbar, 2017). While further validation studies are required, back-of-the-envelope calculations suggest that late season productivity associated with frazil ice may play a significant role in regional carbon cycling.

3.3. Green Colored Frazil Ice Interannual Variability

There is high interannual variability in *Green Frazil Ice Extent* for Antarctica as a whole (Figure 4). Based on a change-point model (PSCBS package for R; segmentByCBS function) (Olshen et al., 2004), there is a statistically significant reduction in March *Green Frazil Ice Extent* after 2012 for the lower and the higher thresholds (1% confidence level; Figure 4). Since sensors on satellites degrade over time, trends in indices derived from band ratios (including our *Green Index*) must be interpreted with caution. However, we used collection 6 MODIS data (Toller et al., 2013) that have been largely corrected for sensor degradation (Casey et al., 2017; Lyapustin et al., 2014). Furthermore, the reduction in *Green Frazil Ice Extent* after 2012 is not observed in all geographical sectors (Figures S10–S13). In short, the reduction is *Green Frazil Ice Extent* after 2012 may be real.

The drivers of interannual variability in *Green Frazil Ice Extent* are not clear. There are no significant correlations (at the 1% confidence level) between *Green Frazil Ice Extent* (examined separately for each threshold and geographical sector) and the SAM, ENSO, and SOI time series between 2003 and 2017. In addition, sea ice production did not decline between 2012 and 2013 (Tamura et al., 2016). *Green Frazil Ice Extent* may be influenced by stochastic processes. For instance, Tamura et al. (2016) found that stochastic icescape dynamics (such as configuration of icebergs, fast ice distribution, and extent of first-year ice) had a larger impact on ice production than large-scale climate modes. These same icescape dynamics, along with katabatic wind speeds, upper ocean physical dynamics, and trace nutrient concentrations, may be the main drivers of *Green Frazil Ice Extent*.

4. Conclusions

Recent studies provide evidence for substantial late summer primary productivity in the Terra Nova Bay and Cape Darnley polynyas (DeJong et al., 2017; Lieser et al., 2015). This water column productivity is associated

with algal accumulation in frazil ice. Since satellite-based chlorophyll maps mask areas with frazil ice, it was previously not known whether frazil ice-associated algal blooms are a local or regional phenomenon. In this study we analyzed daily 500 m resolution MODIS visible spectral band satellite images to identify green frazil ice hot spots and quantify interannual variability in *Green Frazil Ice Extent*. We observed that green frazil ice was concentrated in 11 of the 13 major sea ice production polynyas, supporting the hypothesis that frazil ice-associated algal bloom productivity is ultimately stimulated by strong winds (DeJong et al., 2017). We observed that green frazil ice was present over greater than 300,000 km^2 during March based on the medium threshold, although there was substantial interannual variability that could not be explained by large-scale climate modes. In conclusion, late season frazil ice-associated algal blooms are a major phenomenon in Antarctic polynyas that are not currently accounted for in regional biogeochemical and ecological models.

Acknowledgments
This research was supported by the U.S. NSF (OPP-1142044 to R.B. Dunbar) and NSF Graduate Research Fellowship grant (DGE-114747 to H.B. DeJong). We thank two anonymous reviewers for their valuable feedback. The MODIS and Landsat data are freely available for download courtesy of the NASA Land Processes Distributed Active Archive Center (LP DAAC) at the United States Geological Survey (USGS) Earth Resources Observation and Science (EROS) Center (https://lpdaac.usgs.gov).

References

Arrigo, K. R., & McClain, C. R. (1994). Spring phytoplankton production in the Western Ross Sea. *Science, 266*(5183), 261–263. https://doi.org/10.1126/science.266.5183.261

Arrigo, K. R., van Dijken, G., & Long, M. (2008). Coastal Southern Ocean: A strong anthropogenic CO_2 sink. *Geophysical Research Letters, 35*, L21602. https://doi.org/10.1029/2008GL035624

Arrigo, K. R., van Dijken, G. L., & Bushinsky, S. (2008). Primary production in the Southern Ocean, 1997-2006. *Journal of Geophysical Research, 113*, C08004. https://doi.org/10.1029/2007JC004551

Arrigo, K. R., van Dijken, G. L., & Strong, A. L. (2015). Environmental controls of marine productivity hot spots around Antarctica. *Journal of Geophysical Research, Oceans, 120*, 5545–5565. https://doi.org/10.1002/2015JC010888

Arrigo, K. R., Weiss, A. M., & Smith, W. O. (1998). Physical forcing of phytoplankton dynamics in the southwestern Ross Sea. *Journal of Geophysical Research, 103*, 1007–1021. https://doi.org/10.1029/97JC02326

Bromwich, D. H. (1989). An extraordinary katabatic wind regime at Terra Nova Bay, Antarctica. *Monthly Weather Review, 117*(3), 688–695. https://doi.org/10.1175/1520-0493(1989)117%3C0688:AEKWRA%3E2.0.CO;2

Casey, K. A., Polashenski, C. M., Chen, J., & Tedesco, M. (2017). Impact of MODIS sensor calibration updates on Greenland Ice Sheet surface reflectance and albedo trends. *The Cryosphere, 11*(4), 1781–1795. https://doi.org/10.5194/tc-11-1781-2017

DeJong, H. B., & Dunbar, R. B. (2017). Air-sea CO_2 exchange in the Ross Sea, Antarctica. *Journal of Geophysical Research: Oceans., 122*, 8167–8181. https://doi.org/10.1002/2017JC012853

DeJong, H. B., Dunbar, R. B., Koweek, D. A., Mucciarone, D. A., Bercovici, S. K., & Hansell, D. A. (2017). Net community production and carbon export during the late summer in the Ross Sea, Antarctica. *Global Biogeochemical Cycles, 31*, 473–491. https://doi.org/10.1002/2016GB005417

Esaias, W. E., Abbott, M. R., Barton, I., Brown, O. B., Campbell, J. W., Carder, K. L., … Minnett, P. J. (1998). An overview of MODIS capabilities for ocean science observations. *IEEE Transactions on Geoscience and Remote Sensing, 36*(4), 1250–1265. https://doi.org/10.1109/36.701076

Gower, J., & King, S. (2007). An Antarctic ice-related "superbloom" observed with the MERIS satellite imager. *Geophysical Research Letters, 34*, L15501. https://doi.org/10.1029/2007GL029638

Gower, J. F. R., & King, S. A. (2013). An apparent continuing increase in Antarctic "superblooms" in ice. *Remote Sensing Letters, 4*(3), 261–269. https://doi.org/10.1080/2150704X.2012.720395

Grenfell, T. C. (1983). A theoretical model of the optical properties of sea ice in the visible and near infrared. *Journal of Geophysical Research, 88*, 9723–9735. https://doi.org/10.1029/JC088iC14p09723

Grenfell, T. C. (1991). A radiative transfer model for sea ice with vertical structure variations. *Journal of Geophysical Research, 96*, 16,991–17,001. https://doi.org/10.1029/91JC01595

Hu, C. (2011). An empirical approach to derive MODIS ocean color patterns under severe Sun glint. *Geophysical Research Letters, 38*, L01603. https://doi.org/10.1029/2010GL045422

Jacobs, S. S., Amos, A. F., & Bruchhausen, P. M. (1970). Ross Sea oceanography and Antarctic bottom water formation. *Deep Sea Research and Oceanographic Abstracts, 17*(6), 935–962. https://doi.org/10.1016/0011-7471(70)90046-X

Lieser, J. L., Curran, M. A. J., Bowie, A. R., Davidson, A. T., Doust, S. J., Fraser, A. D., … Wright, S. W. (2015). Antarctic slush-ice algal accumulation not quantified through conventional satellite imagery: Beware the ice of March. *The Cryosphere Discussions, 9*(6), 6187–6222. https://doi.org/10.5194/tcd-9-6187-2015

Long, M. C., Dunbar, R. B., Tortell, P. D., Smith, W. O., Mucciarone, D. A., & Ditullio, G. R. (2011). Vertical structure, seasonal drawdown, and net community production in the Ross Sea, Antarctica. *Journal of Geophysical Research, 116*, C10029. https://doi.org/10.1029/2009JC005954

Lyapustin, A., Wang, Y., Xiong, X., Meister, G., Platnick, S., Levy, R., … Angal, A. (2014). Scientific impact of MODIS C5 calibration degradation and C6+ improvements. *Atmospheric Measurement Techniques, 7*(12), 4353–4365. https://doi.org/10.5194/amt-7-4353-2014

Marshall, G. J. (2003). Trends in the southern annular mode from observations and reanalyses. *Journal of Climate, 16*(24), 4134–4143. https://doi.org/10.1175/1520-0442%20(2003)016%3C4134:TITSAM%3E2.0.CO;2

Mu, L., Stammerjohn, S. E., Lowry, K. E., & Yager, P. L. (2014). Spatial variability of surface pCO_2 and air-sea CO_2 flux in the Amundsen Sea polynya, Antarctica. *Elementa, 2*, 36. https://doi.org/10.12952/journal.elementa.000036

Ohshima, K. I., Fukamachi, Y., Williams, G. D., Nihashi, S., Roquet, F., Kitade, Y., … Wakatsuchi, M. (2013). Antarctic Bottom Water production by intense sea-ice formation in the Cape Darnley polynya. *Nature Geoscience, 6*(3), 235–240. https://doi.org/10.1038/ngeo1738

Olshen, A. B., Venkatraman, E. S., Lucito, R., & Wigler, M. (2004). Circular binary segmentation for the analysis of array-based DNA copy number data. *Biostatistics, 5*(4), 557–572. https://doi.org/10.1093/biostatistics/kxh008

Orsi, A. H., Johnson, G. C., & Bullister, J. L. (1999). Circulation, mixing, and production of Antarctic Bottom Water. *Progress in Oceanography, 43*(1), 55–109. https://doi.org/10.1016/S0079-6611(99)00004-X

Parish, T. R., & Bromwich, D. H. (1987). The surface windfield over the Antarctic ice sheets. *Nature, 328*(6125), 51–54. https://doi.org/10.1038/328051a0

Perovich, D. K. (1996). The optical properties of sea ice. *CRREL Monograph*, 96–91.

Rouse, J. W., Haas, R. H., Schell, J. A., & Deering, D. W. (1973). Monitoring vegetation Systems in the Great Okains with ERTS. *Third Earth Resources Technology Satellite-1 Symposium, 1*, 325–333.

Sanz Rodrigo, J., Buchlin, J. M., van Beeck, J., Lenaerts, J. T. M., & van den Broeke, M. R. (2013). Evaluation of the antarctic surface wind climate from ERA reanalyses and RACMO2/ANT simulations based on automatic weather stations. *Climate Dynamics, 40*(1-2), 353–376. https://doi.org/10.1007/s00382-012-1396-y

Smith, W. O., & Gordon, L. I. (1997). Hyperproductivity of the Ross Sea (Antarctica) polynya during austral spring. *Geophysical Research Letters, 24*, 233–236. https://doi.org/10.1029/96GL03926

Smith, W. O., Marra, J., Hiscock, M. R., & Barber, R. T. (2000). The seasonal cycle of phytoplankton biomass and primary productivity in the Ross Sea, Antarctica. *Deep Sea Research Part II, 47*(15-16), 3119–3140. https://doi.org/10.1016/S0967-0645(00)00061-8

Smith, W. O., Nelson, D. M., DiTullio, G. R., & Leventer, A. R. (1996). Temporal and spatial patterns in the Ross Sea: Phytoplankton biomass, elemental composition, productivity and growth rates. *Journal of Geophysical Research, 101*, 18,455–18,465. https://doi.org/10.1029/96JC01304

Sweeney, C. (2003). The annual cycle of surface water CO_2 and O_2 in the Ross Sea : A model for gas exchange on the continental shelves of Antarctica. In G. R. DiTullio & R. B. Dunbar (Eds.), *Biogeochemistry of the Ross Sea, Antarctic research series* (Vol. 78, pp. 295–310). Washington, DC: American Geophysical Union. https://doi.org/10.1029/078ARS19

Tamura, T., Ohshima, K. I., Fraser, A. D., & Williams, G. D. (2016). Sea ice production variability in Antarctic coastal polynyas. *Journal of Geophysical Research, 121*, 2967–2979. https://doi.org/10.1002/2015JC011537

Toller, G., Xiong, X., Sun, J., Wenny, B. N., Geng, X., Kuyper, J., … Wu, A. (2013). Terra and Aqua moderate-resolution imaging spectroradiometer collection 6 level 1B algorithm. *Journal of Applied Remote Sensing, 7*(1), 073557. https://doi.org/10.1117/1.JRS.7.073557

Vermote, E. F., Roger, J. C., & Ray, J. P. (2015). MOD09GA MODIS/Terra surface reflectance daily L2G global 1 km and 500 m SIN grid V006. NASA EOSDIS Land Processes DAAC. https://doi.org/10.5067/modis/mod09ga.006

Wessel, P., & Smith, W. H. F. (1996). A global, self-consistent, hierarchical, high-resolution shoreline database. *Journal of Geophysical Research, 101*, 8741–8743. https://doi.org/10.1029/96JB00104

Wolter, K., & Timlin, M. S. (1993). Monitoring ENSO in COADS with a seasonally adjusted principal component index. In *Proceedings of the 17th climate diagnostics workshop* (pp. 52–57). Norman, OK: University of Oklahoma.

Wolter, K., & Timlin, M. S. (1998). Measuring the strength of ENSO events: How does 1997/98 rank? *Weather, 53*(9), 315–324. https://doi.org/10.1002/j.1477-8696.1998.tb06408.x

Yager, P., Sherrell, R., Stammerjohn, S., Ducklow, H., Schofield, O., Ingall, E., … van Dijken, G. (2016). A carbon budget for the Amundsen Sea polynya, Antarctica: Estimating net community production and export in a highly productive polar ecosystem. *Elementa, 4*, 140. https://doi.org/10.12952/journal.elementa.000140